SEMATECH

TECHNOLOGY TRANSFER

Characterization & Calibration of a BIT/RGA for Use as a Plasma Processing Diagnostic

93041615A-XFR

August 12, 1993

SEMATECH CONFIDENTIAL

SEMATECH CONFIDENTIAL

August 15, 1995

SEMATECH-XFR

for use as a Plasma Processing Diagnostic
Characterization & Calibration of a BITMCA

TECHNOLOGY TRANSFER

SEMATECH

SEMATECH TRANSFERABLE

To facilitate the flow of information while optimizing use of resources, this document is made available "as is."

August 12, 1993

93041615A-XFR

Characterization & Calibration of a BIT/RGA for Use as a Plasma Processing Diagnostic

Abstract: The purpose of this project was to characterize a mass spectrometer with an ion energy analyzer so it could be used as a plasma diagnostic tool on commercial semiconductor etching reactors. This investigation of the bulk ion temperature/residual gas analyzer (BIT/RGA) as a possible diagnostic device emphasized the application of monitoring ion energies. The document presents the results obtained from the BIT/RGA installed at National Institute of Standards and Technology (NIST) and those obtained from the system installed at SEMATECH.

Key Words: Spectrometers, Calibration, Equipment Characterization

Thrust Area: Etch/Modeling

Norman Williams
Author
Norman Williams

Linda Wilson
Technology Transfer
Team Leader
Linda Wilson

Inquiries should be directed to Technology Transfer (512) 356-SEMA

Characterization and Calibration of a BIT/RGA for Use as a Plasma Processing Diagnostic

James K. Olthoff
Richard J. Van Brunt

U.S. DEPARTMENT OF COMMERCE
National Institute of Standards and Technology
Electronics and Electrical Engineering Laboratory
Electricity Division
Gaithersburg, MD 20899

Prepared for
SEMATECH, Austin, TX
NIST PRSC CAL CONTRACT

September 1991

Table of Contents

Table of Contents

CONTENTS

1 Introduction

Ion bombardment plays a crucial role in the anisotropic etching of semiconductor materials [1]. It has been shown that etching anisotropy and etching rates increase with increasing ion flux and ion kinetic energy [2]. Generally three processes are proposed to explain the role of ion bombardment in the etching process [3]:

1) Dissociation of etching gases into reactive fragments may occur preferentially at defect sites produced by ion bombardment.

2) Ion collisions may cause an adsorbed molecule to dissociate in situations where this would normally not occur.

3) Ion bombardment may remove monolayers of adsorbed gases thus exposing a clean surface required for some dissociative chemisorption reactions.

A significant amount of research has been performed over the past 15–20 years to understand more fully the details of the processes listed above and to quantify the role of ion bombardment in the etch process. As semiconductor manufacturers work towards producing chips with 0.25 μm size features, the need to characterize and control the etching process will make it necessary to go beyond our present knowledge of the mechanisms of ion flux-assisted etching. In order to provide the control required for the production of future semiconductor devices it has been suggested that methods must be developed to ensure that bombarding ions exhibit narrow kinetic-energy distributions and that ion fluxes and mean energies are controllable [4]. The first step toward meeting these demands is to develop the methods for monitoring bombarding ion currents and energies, and to determine how these parameters vary with plasma conditions.

A device under consideration to monitor ion current and ion energy distributions is an electrostatic energy filter followed by a mass spectrometer. When applied to a plasma reactor, ions are usually sampled through a small hole in the grounded electrodes. Coburn and co-workers [5] are generally credited with being the first researchers to employ this type of device to monitor ions bombarding surfaces exposed to an rf discharge. They then extended their research to develop a technique for determining plasma sheath potentials from measured ion energy distributions [6] and to determine the dependence of ion energies on the frequency of the applied rf voltage [7].

Green *et al.* [8] have utilized an instrument similar to Coburn's except the ion energy filter is an on-axis cylindrical mirror analyzer (CMA) [9]. They measured ion energy distributions for Ar^+ and ArH^+ sampled from an rf argon discharge and observed a broadening of energy distributions with increasing pressure. Ingram and Braithwaite [10] observed similar broadening of ion energy distributions from argon plasmas by utilizing a retarding potential analyzer (RPA) but with no mass analysis.

Liu *et al.* [11] have used a modified RPA to show that momentum transfer scattering in the sheath is essential to produce ions with a significant velocity component parallel to the surface under bombardment.

Other researchers have utilized retarding potential analyzers combined with a mass spectrometer. Thompson and co-workers [12] have reported some of the first energy distributions measured for halogen-containing gases commonly used in etching processes. More recently, Toups and Ernie [13] have identified the ratio of the reactor gas pressure to the frequency of the applied voltage as a critical parameter in determining the shapes of the ion energy distributions of Ar^+.

All of the previously mentioned experiments were performed by analyzing ions that were sampled through a small orifice in the grounded electrodes of different parallel plate reactors. In an etching reactor the ions of interest are normally those striking the semiconductor wafer which is mounted on the powered electrode. Few measurements have been made of the ion flux striking the powered electrode because of the increased experimental difficulties caused by the ever-present rf signal. However, recently-designed experiments have allowed preliminary measurements of the ions striking the powered electrode. Kuypers and Hopman [14] measured ion energy distributions at the powered electrode of a cylindrical electrode discharge chamber by utilizing optical fibers to isolate the ion current signals from the rf voltage. Mannenschijn *et al.* [15] performed a similar experiment in a parallel plate discharge by using a low-pass filter for electrical isolation. Wild and Koidal [16] eliminated the necessity for the isolation of the ion signal from the rf voltage by reversing the electrical geometry of the normal parallel plate reaction and by powering the chamber itself with only a small grounded electrode from which to sample ions. This changes the sheath potentials such that the grounded electrode behaves as the powered electrode with respect to ion bombardment energies.

All of these experiments exhibited results in reasonable agreement with each other. As anticipated the measured distributions were similar to those observed through the grounded electrodes except the energy ranges were much higher due to the larger sheath potentials at the powered electrodes. While the measurement of ion energies at the powered electrode provides information about the energies of the ion flux striking the etching wafer directly, the electrical complications and the lack of mass analysis presently make these techniques unfeasible for application on commercial reactors.

2 Technical Overview

2.1 Introduction

The basic goal of this project was to characterize a mass spectrometer with an ion energy analyzer such that the instrument could be used as a plasma diagnostic tool

on commercial semiconductor etching reactors. The instrument measures the kinetic-energy distributions of ions sampled from a plasma and monitors concentrations of various neutral by-products in the reactor gas. Because of these applications this type of instrument is sometimes referred to as a Bulk Ion Temperature/Residual Gas Analyzer (or BIT/RGA). Our investigation of the BIT/RGA as a possible diagnostic device emphasized the application of monitoring ion energies since a significant amount of research related to using a mass spectrometer to monitor neutral species in the plasma has been done previously [17–19].

Before a BIT/RGA could be used as a control diagnostic, its operation and performance under well-defined conditions needed to be characterized. This basic set of knowledge is essential in order to understand and to have confidence in the data being acquired from an etching plasma. The characterization had to determine:

- the ability of the instrument to measure the kinetic energy of ions sampled from low pressure plasmas;
- how well the instrument measures the energy of the ions (particularly at low energies);
- the effects of the instrumental configuration (such as sampling geometry, orifice size, etc.) upon the BIT/RGA performance;
- the detection sensitivity of the instrument;
- the time required to acquire the desired data;
- the reproducibility of the data;
- the effects of changes of instrumental parameters (such as pole bias, resolution setting, pass energy, etc.) on the measured data; and,
- the effects of exposure to corrosive gases on the instrument.

At the outset of the project it was assumed that time and repetitive exposure to corrosive etching gases would affect the response of the BIT/RGA. Therefore, in addition to addressing the issues listed above, a primary goal of this project was to develop a calibration procedure for the BIT/RGA in order to verify and adjust for any changes in performance.

The information presented in this report is a result of our attempt to characterize one particular BIT/RGA instrument. Other BIT/RGA instruments with similar capabilities are available from other manufacturers, but obviously the cost involved in characterizing more than one would be prohibitive. Thus the results presented here must be viewed in light of the specific instrument used, and may or may not be applicable to other BIT/RGA's.

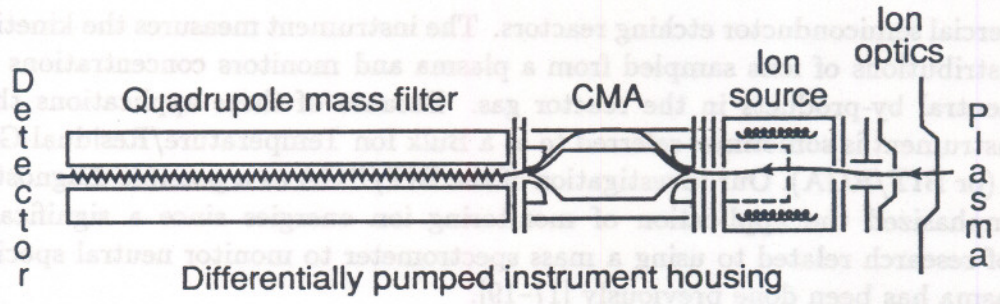

Figure 1. Schematic diagram of the CMA quadrupole mass spectrometer instrument.

2.2 The BIT/RGA

The BIT/RGA chosen for use in this project is an SXP300H/CMA quadrupole mass analyzer equipped with a cylindrical mirror ion energy filter and is manufactured by Fisons Analytical, Inc.[1] A schematic diagram of the SXP300H/CMA is shown in Figure 1. Ions are sampled from the plasma through a small aperture (50 μm – 200 μm), are energy analyzed by a cylindrical mirror analyzer (CMA) [9], and then mass analyzed by a quadrupole mass spectrometer. Neutrals may be monitored in a similar manner except they must be ionized in the electron impact source preceding the CMA.

When installed in its stainless steel vacuum chamber, the BIT/RGA is approximately a meter in length and mounts onto a 15.24-cm (6-inch) conflat flange. Special mounting flanges have been designed to allow the instrument to be mounted onto smaller ports which are more common on commercial reactors. Differential pumping is provided by a 230 liter/second turbo pump and the pressure is monitored by a high vacuum gauge mounted to a 7-cm ($2\frac{3}{4}$-inch) conflat. The instrumental assembly is quite large and heavy and is not generally self-supporting; however, the BIT/RGA may be mounted in practically any orientation if the required mounting hardware is added.

The mass spectrometer portion of the instrument has a stated range of 1–300 atomic mass units (AMU) with a mass resolution of better than 1 AMU (Full Width at Half Maxuimum) over the entire mass range. Mass spectra (i.e., intensity versus mass plots) may be obtained by computer control in either raw or analyzed form. The stated detection sensitivity for neutral detection is 1 ppm but a mass scan configured for maximum sensitivity is quite slow and may require as long as 15–20 minutes depending on the required signal-to-noise ratio. Since this instrument contains both a mass and an energy filter, it is not possible to operate one without the other. One may therefore obtain mass spectra only for specified ion energies. This has little

[1]The identification of commercial materials and their sources is made to describe the experiment adequately. In no case does this identification imply recommendation by the National Institute of Standards and Technology, nor does it imply that the instrument is the best available.

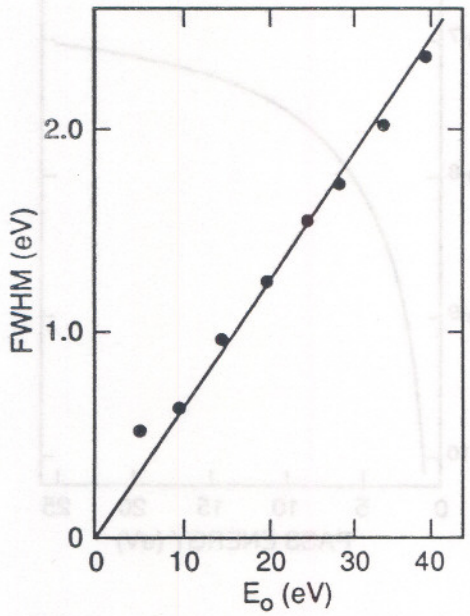

Figure 2. Plot of the energy resolution (FWHM) of the CMA as a function of pass energy (E_0). Figure obtained from the SXP300H/CMA operator's manual.

effect on the analysis of neutrals ionized in the electron impact source, but may have a substantial effect on the mass analysis of ions produced in a plasma since different ions may have vastly different kinetic-energy distributions.

The CMA is an electrostatic ion-energy filter which is compact and allows for "on-axis" ion selection. The energy resolution of the CMA is determined by the energy of the ions as they pass through the analyzer (the pass energy). During an energy scan, all ions are accelerated (or de-accelerated) to the same pass energy so that the energy resolution is independent of initial ion energy. As can be seen in Figure 2, the energy resolution is linearly dependent ($\Delta E/E_0 \cong 0.063$) on the pass energy down to 10 eV. Slightly better energy resolution can be obtained by further reducing the pass energy to 5 eV but, as can be seen in Figure 3 a significant loss in detection sensitivity also occurs. For the data presented in this report, the pass energy was set at 10 eV and the resolution was confirmed to be 0.5 eV (FWHM) by analysis of an ion beam with a well-defined distribution of kinetic energies.

2.3 The BIT/RGA as Installed at NIST

Much of the characterization of the BIT/RGA was performed with the instrument installed on a GEC[2] rf reference cell [20]. The reference cell is a parallel plate research reactor with 10.2 cm (4-inch) aluminum electrodes with an interelectrode spacing of

[2]Gaseous Electronics Conference

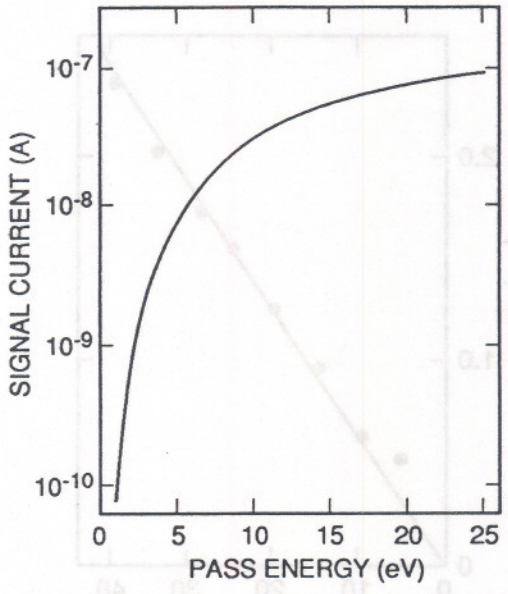

Figure 3. Signal intensity as a function of pass energy for the CMA. Figure obtained from the SXP300H/CMA operator's manual.

2.54 cm (1 inch) and is shown schematically in Figure 4. The plasmas were generally low power (applied peak-to-peak voltage $\leq$ 200 V) argon or argon/oxygen discharges using 99.999 % argon and 99.9 % O_2. Gases were supplied to the plasma through a showerhead arrangement of small holes in the grounded upper electrode. The lower electrode was capacitively powered at 13.56 MHz.

The GEC rf reference cell was used for this investigation because of its simple design, and because it is currently the "test-bed" reactor for a program which is attempting to characterize an rf discharge. During the course of this program, the GEC reference cell has been electrically characterized by several laboratories and is being further investigated by mass spectrometric, optical emission, and electric probe techniques. The fact that the performance of the GEC cell has been thoroughly investigated makes it well suited for use in characterizing the BIT/RGA.

The BIT/RGA was attached to the cell through a side 15.24 cm (6-inch) conflat port. A bellows assembly allowed the distance between the sampling orifice and the edge of the electrodes to be varied from 0–10 cm. A schematic diagram showing the orientation of the BIT/RGA to the electrode assembly is shown in Figure 5. Sampling ions from the side of the plasma (rather than through a grounded electrode) more closely resembles the sampling geometry that would be used to install the BIT/RGA on commercial etching reactors.

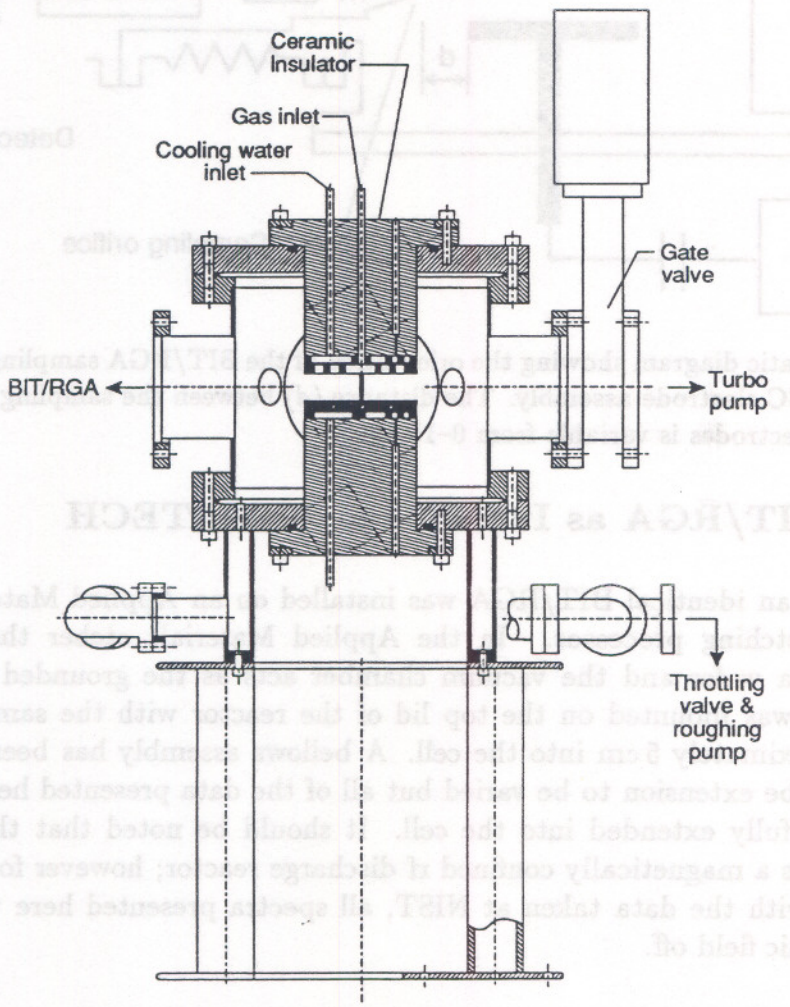

Figure 4. Schematic diagram of the GEC rf reference reactor.

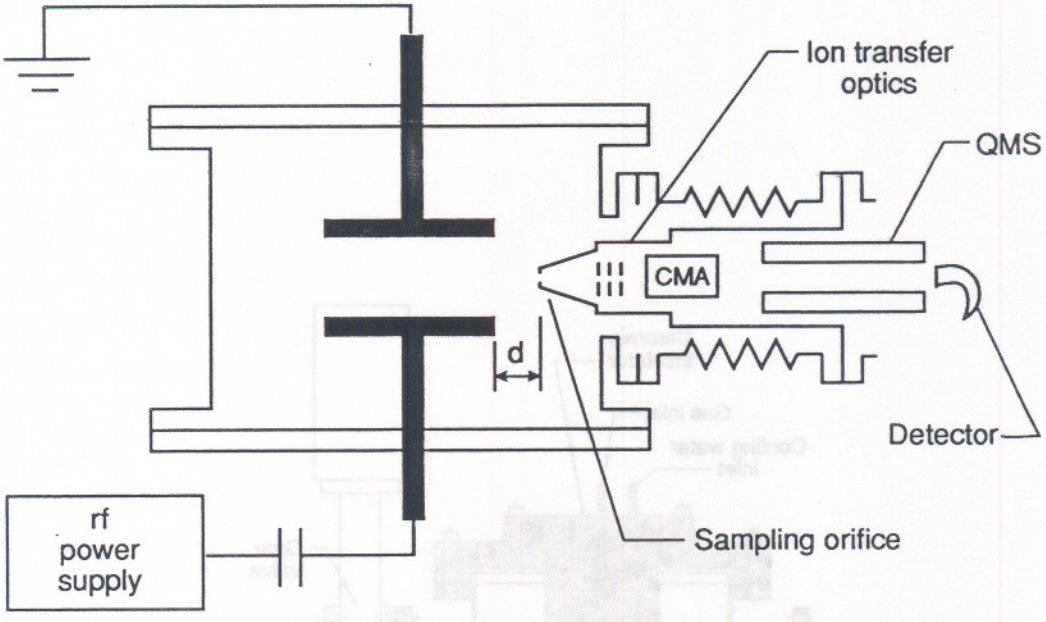

Figure 5. Schematic diagram showing the orientation of the BIT/RGA sampling cone with respect to the GEC electrode assembly. The distance (d) between the sampling orifice and the edge of the electrodes is variable from 0–10 cm.

2.4 The BIT/RGA as Installed at SEMATECH

For comparison an identical BIT/RGA was installed on an Applied Materials 5000 semiconductor etching processor. In the Applied Materials etcher the powered electrode holds a wafer and the vacuum chamber acts as the grounded electrode. The BIT/RGA was mounted on the top lid of the reactor with the sampling core extending approximately 5 cm into the cell. A bellows assembly has been designed to allow the probe extension to be varied but all of the data presented here is made with the probe fully extended into the cell. It should be noted that the Applied Materials 5000 is a magnetically confined rf discharge reactor; however for purposes of comparison with the data taken at NIST, all spectra presented here were made with the magnetic field off.

3 Instrument Characterization

3.1 General Data Characterization

Figure 6 shows a sample mass spectrum of ions extracted from an oxygen discharge. The resolution is better than 1 AMU (FWHM) over the entire mass range. The resolution and relative peak heights may be changed by adjustment of various

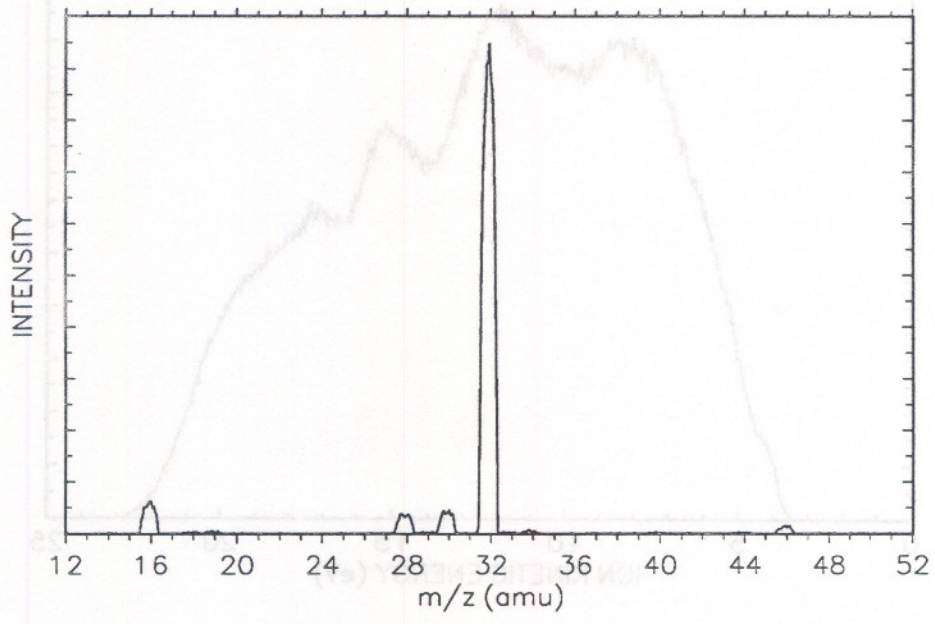

Figure 6. Typical mass spectrum of ions sampled from an O_2 discharge in the GEC reference cell with the energy filter set at 22 eV.

quadrupole settings. The instrument may be adjusted to provide electron impact mass spectra of neutral molecules whose relative intensities agree with reference spectra [21]. It should be pointed out again that the kinetic-energy setting of the CMA may significantly affect the mass spectra of ions samples from a plasma. This will be discussed further in section 3.3 where the difference in kinetic-energy distributions for different ions is investigated.

Figure 7 shows a raw kinetic-energy distribution for Ar^+ ions sampled from a 13.3 Pa (100 mTorr) argon discharge ($V_{pp} = 200$ V) with $d = 0$. Two features of the distribution are immediately obvious. The first is that no ion signal is detected at energies below ~ 3.5 eV. This apparent low energy cut-off, as shown from tests performed here, can be attributed to charge accumulation on the inner surfaces of the sampling cone. This effect will be discussed in greater detail in the next subsection. Compensation for this effect has been made on kinetic-energy distributions presented in this section. The other obvious features in Figure 7 are the structure or secondary maxima which are evident in the ion energy distribution near 8, 12, 15, and 17 eV. These maxima are due to collisional interactions in the plasma sheath and are discussed in more detail in section 3.3.

The shape and reproducibility of the ion energy distributions may be modified by adjustment of the BIT/RGA instrument parameters such as pass energy and scan times. Increasing the pass energy from 10 eV to 20 eV will decrease the energy resolution to ~ 1 eV and obscures some of the observed structure. Decreasing the pass energy to 5 eV slightly improves the energy resolution but significantly lowers

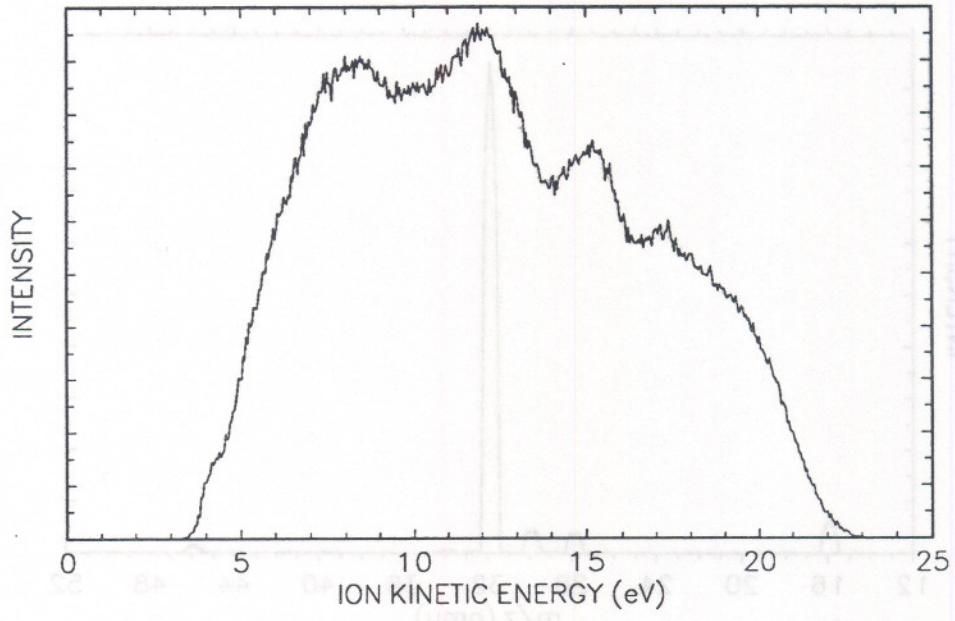

Figure 7. Raw kinetic-energy distribution acquired from an argon plasma by the SXP300H/CMA. The pressure is 13.3 Pa (100 mTorr), V_{pp}=200 V, and d=0.

the signal level. The rate at which the kinetic energy is scanned can affect the reproducibility of the kinetic-energy spectra. Fast scans ($\sim$ 1 second) have less scan-to-scan reproducibility than longer scans ($\sim$ 10 seconds or larger). Thus for conditions where signal levels were high and lower sensitivity settings (with faster scan rates) were used, the amount of signal averaging would be increased in order to slow the scan rate. For example, the spectrum in Figure 7 was taken with an average setting of 16. This improved the signal-to-noise ratio and also improved the reproducibility of the data.

Even when taking care to run the instrument in the most reproducible mode, the kinetic-energy spectra exhibit fluctuation in day-to-day operation, particularly in the low energy portions of the spectra. Figure 8 shows two Ar^+ kinetic-energy distributions taken on different days. While the general shapes are the same, the magnitudes at low energies are quite different. Investigations performed on a uniform-field drift tube at NIST indicate that these changes are probably due to variations in the plasma. The fluctuations in ion signal provide an indication of our present capability to reproduce an rf discharge, and also indicate the possible application of the BIT/RGA to detect changes in the plasma which may not be observable by other diagnostics.

An additional concern was whether the response of the BIT/RGA would change with repeated exposures to plasmas containing corrosive gases such as Cl_2. An experiment was performed on the Applied Materials 5000 etching reactor to monitor the response of the BIT/RGA to successive exposures to a Cl_2 plasma. Figure 9 shows three Ar^+

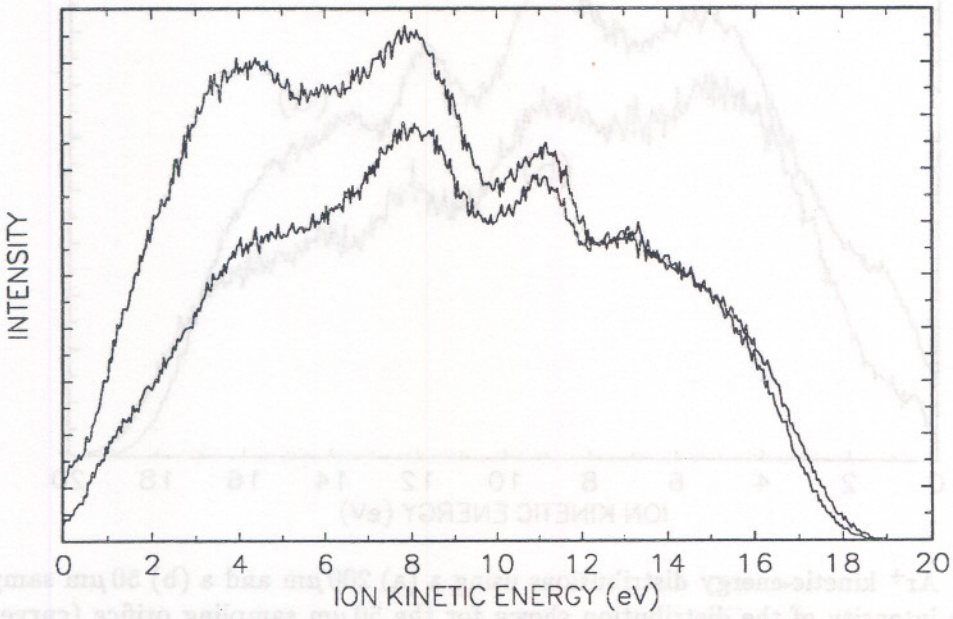

Figure 8. Ar^+ kinetic-energy distribution acquired on different days.

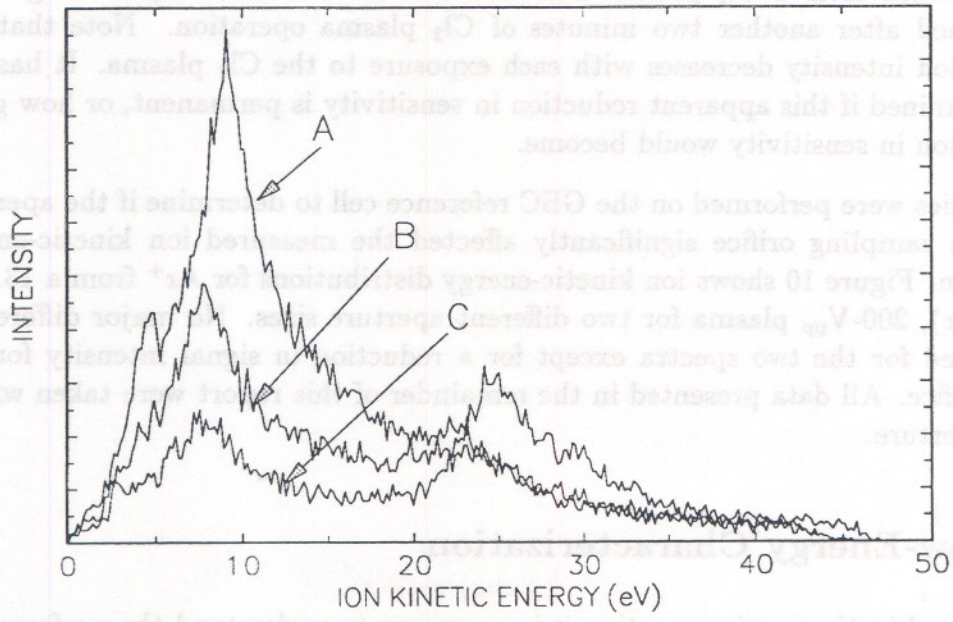

Figure 9. Plot showing the effects of repetitive exposure to Cl_2 plasmas on the measured Ar^+ ion energy distributions. See text for further explanation.

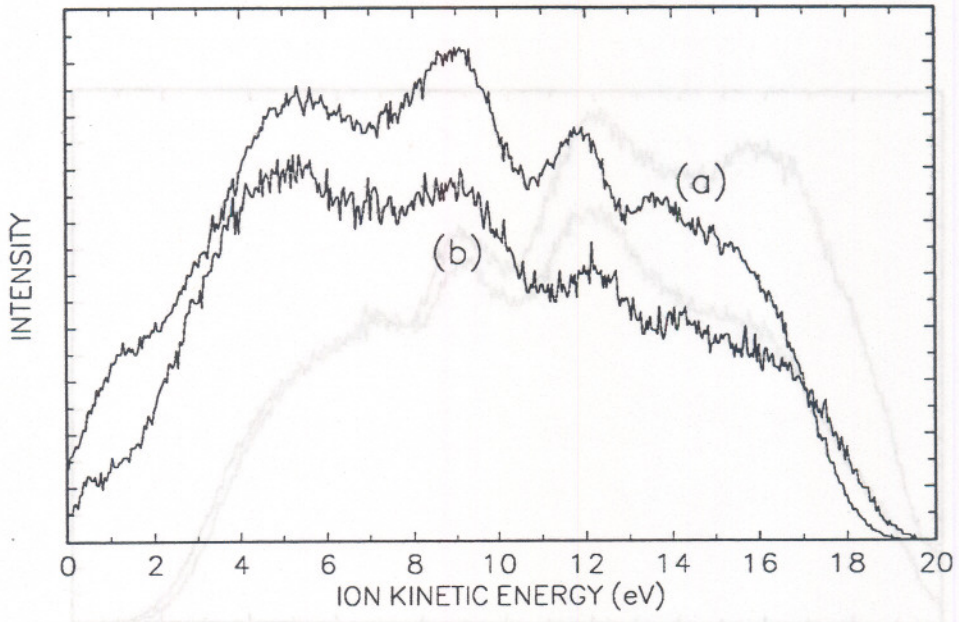

Figure 10. Ar^+ kinetic-energy distributions using a (a) 200 μm and a (b) 50 μm sampling orifice. The intensity of the distribution shown for the 50 μm sampling orifice (curve (b)) has been multiplied by 3.5 to allow easier comparison.

kinetic-energy spectra from an argon plasma. Figure 9a is a spectrum obtained before the BIT/RGA had been exposed to an etching plasma. Figure 9b shows another Ar^+ spectrum taken after a Cl_2 plasma had been run for two minutes, and Figure 9c was obtained after another two minutes of Cl_2 plasma operation. Note that the measured ion intensity decreases with each exposure to the Cl_2 plasma. It has not been determined if this apparent reduction in sensitivity is permanent, or how great the reduction in sensitivity would become.

Other studies were performed on the GEC reference cell to determine if the aperture size of the sampling orifice significantly affected the measured ion kinetic-energy distribution. Figure 10 shows ion kinetic-energy distributions for Ar^+ from a 13.3 Pa (100-mTorr), 200-V_{pp} plasma for two different aperture sizes. No major differences are observed for the two spectra except for a reduction in signal intensity for the smaller orifice. All data presented in the remainder of this report were taken with a 200 μm aperture.

3.2 Low-Energy Characterization

As mentioned in the previous section it is necessary to understand the performance of the BIT/RGA at low energies. The fact that no ion signal is observed below a certain kinetic-energy threshold (see Figure 7) is not in agreement with other ion energy measurements from argon plasmas [11, 13] in the sense that previous data

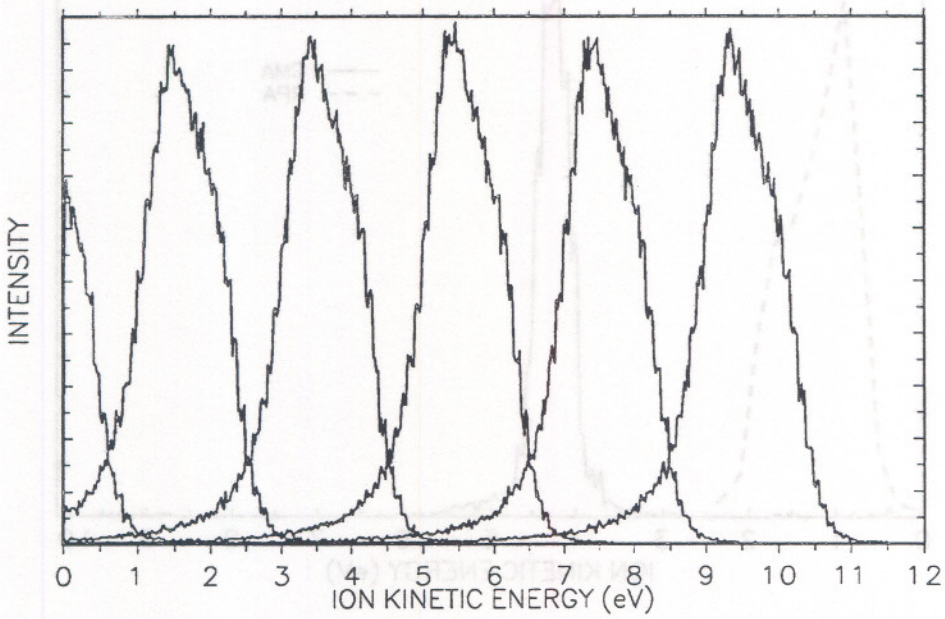

Figure 11. Ion kinetic-energy distribution for Ar^+ ions produced from static argon gas in the BIT/RGA ion source by electron impact. The source potential setting was varied from 0–10 volts.

show finite ion signals down to zero energy. It had to be determined if this apparent threshold was due to a "shift" of the energy scale or to a low-energy "cut-off" (i.e., discrimination of low-energy ions). To investigate this behavior and to aid in the development of a procedure for calibration of the energy analyzer, the BIT/RGA was installed onto a uniform-field drift tube at NIST.

The drift tube consists of a 28-cm long tube made up of 20 stacked stainless steel rings [22]. By applying cascaded voltages with equal potential differences to the rings a uniform electric field is produced along the axis of the tube. A potassium ion source (K^+) is mounted at one end of the drift tube such that ions are accelerated down the tube and into the BIT/RGA. If the drift tube is under vacuum then the measured ion energies will exhibit a distribution which is characterized by the ion source potential, the ion source energy spread, and the energy resolution of the BIT/RGA. If the drift tube is filled with a buffer gas then the measured ion energies will exhibit a distribution which is dependent upon the ratio of the electric field and the gas number density (E/N). These distributions have been predicted by theory [23, 24].

To determine if the low-energy threshold observed in Figure 6 was a result of CMA performance, kinetic-energy distributions were measured for argon ions created in the electron-impact source of the BIT/RGA. Figure 11 shows the distributions for six different source potentials ranging from 0–10 V. Ions are clearly observed with equal intensity over the entire energy range thus indicating that the CMA is not the source of the low-energy threshold. It should be noted that the broad, asymmetric

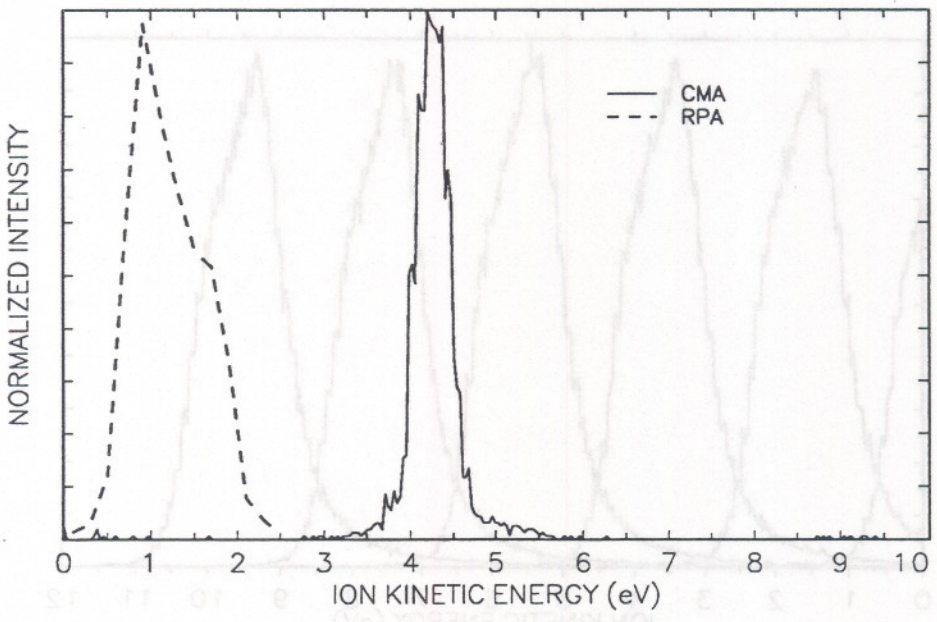

Figure 12. Kinetic energy distributions for K^+ ions produced in the drift tube ion source at 2.9 volts. Distributions are shown as measured by the CMA and by a retarding potential analyzer technique.

energy profiles exhibited in Figure 11 are due primarily to the characteristics of the electron-impact ion source.

However, when the K^+ ion source potential on the drift tube was set at 2.9 V, the CMA measured an ion energy distribution with a peak at 4.2 eV (see Figure 12). The cone of the BIT/RGA was then slightly modified such that it could be used as a retarding potential analyzer [13]. By measuring the ion current striking the cone as a function of the cone voltage, a rough determination of the energy distribution could be made for comparison with that determined by the CMA. Figure 12 shows that the two measurements differ by approximately 3 eV, with respect to each other, and neither agrees with the potential of the K^+ ion source. It is not possible to determine which of these techniques provides the correct distribution since all of them (including measuring the source potential) may suffer from surface charging effects. It does appear obvious however that some form of energy shift is present in these energy measurements.

To investigate further the possibility that the energy distributions measured by the BIT/RGA are shifted, the kinetic-energy distribution for K^+ ions drifting through 100 mTorr of argon were measured for several values of E/N. The data from these measurements are shown in Figure 13. At low E/N the kinetic-energy distributions are nearly maxwellian while as E/N increases the distributions exhibit high energy tails. The shapes of these distributions are in agreement with previous measurements made for cesium ions in argon [23]. However, theory predicts that the distributions

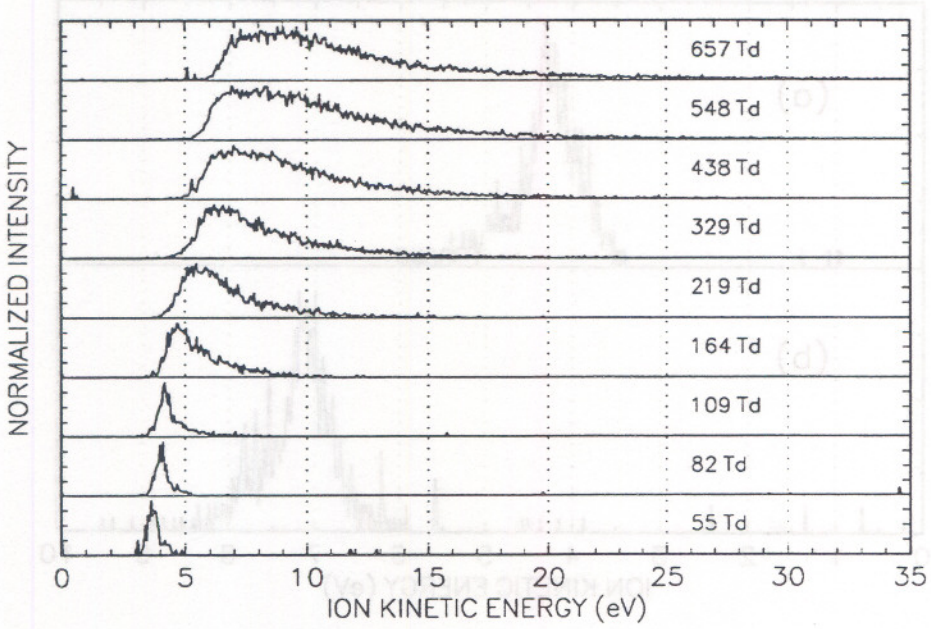

Figure 13. Ion energy distributions for K^+ in argon for different E/N valves in the drift tube (1 Td = 1×10^{-17} Vcm^2).

should contain ions with kinetic energies extending down to 0 eV. The distributions in Figure 13 again indicate the lack of ions at the low-energy end of the distributions. In fact the threshold increases from 3 eV at low E/N values to almost 6 eV for higher E/N values. Since the shapes of the distributions are correct it is unlikely that some instrumental effect causes ions with less than 3 eV kinetic energy to not be detected. This was further proven by configuring the BIT/RGA and the drift tube such that all ions are accelerated by 3 eV into the BIT/RGA. Figure 14 shows such an ion energy distribution as compared with a normal ion energy distribution. The accelerated distribution is shifted 3 eV with no change in its shape. If any energy discrimination were occurring then some modification of the distribution would be observed.

Thus it appears that the lack of low-energy ions in the measured ion energy distributions (as observed in Figure 7) represents a shift in the energy scale of the entire spectrum. This shift is most likely due to surface charging on the interior walls of the sampling cone such that ions are accelerated from the sampling orifice into the ion transfer optics. When we replaced the sampling cone with a different sampling device (with a different shape, aperture size, and surface characteristics) the energy shifts were different, thus supporting the possibility of surface charging near the sampling orifice.

The energy shift is easily compensated when making measurements of ions from an argon plasma since it has been shown that Ar^+ exhibits an ion energy distribution extending down to 0 eV due to charge-exchange collisions in the sheath [11, 13, 16]. Thus the zero-energy point may be determined by locating the Ar^+ signal threshold

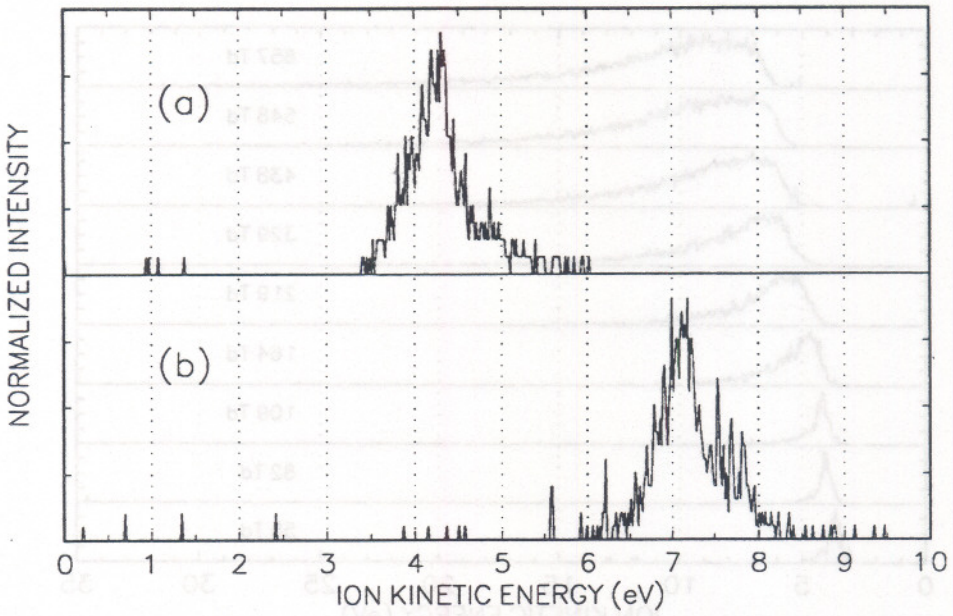

Figure 14. Ion kinetic-energy distributions for K^+ in argon buffer gas with (a) the cone grounded and with (b) the cone biased to accelerate ions into the analyzer by 3 eV (see text).

and then accounting for the energy resolution of the BIT/RGA. This technique was used for all subsequent spectra shown in this report. An extension of this compensation technique to provide an energy calibration of the BIT/RGA will be presented in Section 4.

3.3 Ion Energy Distributions from an Argon Plasma

As discussed earlier, kinetic-energy distributions of ions sampled from argon plasmas have been measured by many researchers [6, 7, 8, 11, 13, 15, 16]. Argon has received such attention because of the reasonably simple chemistry involved in the plasma, and because the cross sections required for modeling the discharge are fairly well known. For these same reasons, an argon plasma represents a useful reference for the characterization of the BIT/RGA and a suitable application to demonstrate the capabilities of the general technique for monitoring a plasma.

In the following subsections kinetic-energy distributions for Ar^+, Ar^{++}, Ar_2^+, and ArH^+ produced in an argon rf discharge will be presented. The kinetic-energy distributions for H_2O^+, a persistent impurity in most vacuum systems, will also be shown. These distributions will be presented as a function of three variables: applied peak-to-peak rf voltage (V_{pp}), the distance between the sampling orifice of the BIT/RGA and the edge of the electrodes (d), and the gas pressure inside the chamber.

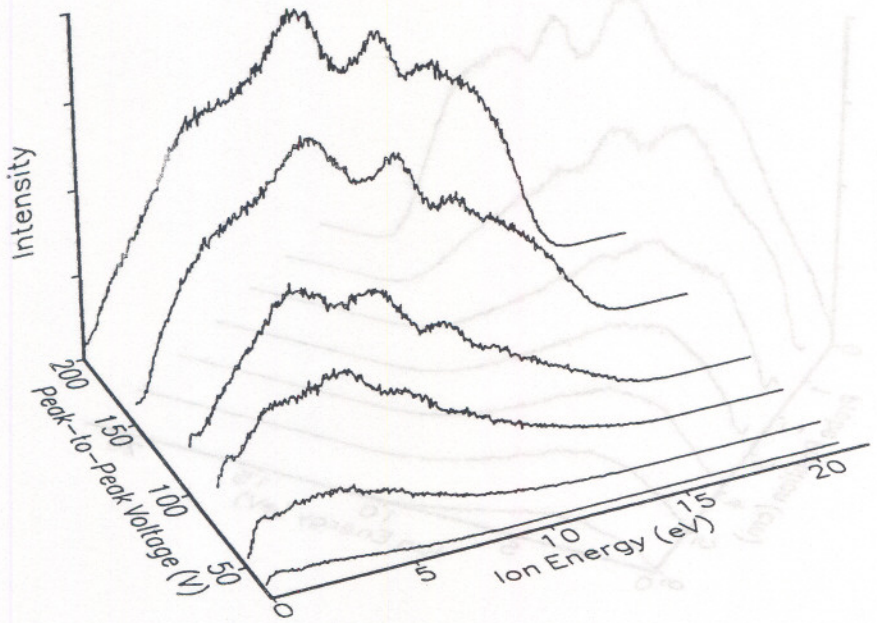

Figure 15. Ar^+ kinetic-energy distributions as a function of peak-to-peak voltage for a 13.3 Pa (100 mTorr) argon plasma with d=0 cm.

3.3.1 Ar^+

Shown in Figure 15 are the ion kinetic-energy distributions for Ar^+ produced in an argon discharge as a function of applied peak-to-peak voltage for the probe positioned at the edge of the electrodes (d=0 cm). At higher voltages the distributions exhibit a structure replete with secondary maxima. Somewhat similar structure has been observed previously in ion-energy distributions sampled through the grounded electrode of parallel plate reactors [11, 13, 16]. This similarity is expected since a sheath develops around the sampling orifice cone when it is positioned near the electrodes so that the grounded cone behaves as an extension of the grounded electrode. The observed structure has been attributed to phase modulation effects associated with formation of low-energy Ar^+ ions by resonant charge transfer in the sheath [16]. As the applied voltage decreases, the structure disappears due to the decreasing thickness of the sheath and subsequently fewer collisions in the sheath.

In the present experiment, the observed ions obtain most of their energy by traversing the sheath potential as they are accelerated from the bulk plasma. If no collisions occur during acceleration and if no new ions are created in the sheath region, then the ion kinetic-energy distributions should exhibit only a narrow energy spread with the maximum observed energy indicating the magnitude of the sheath potential [6]. The broad range of ion energies (0–20 eV) observed in Figure 15 indicates that a significant fraction of the observed Ar^+ is formed initially with low energy by collisional processes in the sheath.

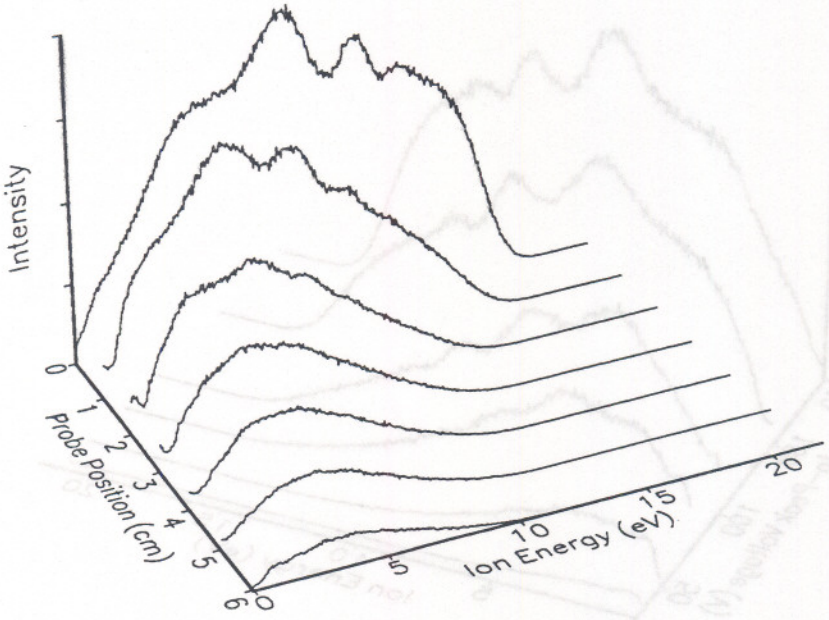

Figure 16. Ar^+ kinetic-energy distributions as a function of probe position for a 13.3 Pa (100 mTorr) argon plasma with V_{pp}=200 V.

Similar behavior in the Ar^+ ion-energy distributions can be observed as a function of the probe position (Figure 16). As the grounded sampling cone is moved away from the electrodes, the secondary maxima quickly disappear, the energy distribution narrows, and the mean ion-energy shifts to lower values. All of these effects are consistent with the diminishing influence of the probe in defining a sheath region near the aperture as d increases. The capability of detecting significant ion flux far from the powered electrode may be an important aspect of using the BIT/RGA as an etching diagnostic. Experiments done with the BIT/RGA on the Applied Materials 5000 indicate that extending the probe into the etching chamber adversely affects the spatial uniformity of the etching process. It may therefore be necessary to sample ions at a point closer to the chamber walls and further from the wafer when the BIT/RGA is used for process control. The uniformity of the plasma was also affected in the GEC cell when the probe was positioned near the edge of the electrodes ($d = 0$). Figure 17 shows an optical emission profile taken at the mid-plane between the electrodes. The spatial dependence of the emission intensity of this transition is modified as the mass spectrometer probe position is changed, thus indicating an influence on the plasma.

Figure 18 shows Ar^+ kinetic-energy distributions as a function of gas pressure from 1.7–13.3 Pa (13–100 mTorr). For pressures ranging from 8–13.3 Pa (60–100 mTorr) there is little observable change in the kinetic-energy distributions. Below 8 Pa (60 mTorr) the distributions change rapidly with pressure as the sheath region moves across the sampling orifice. At 1.7 Pa (13 mTorr) the orifice is sampling ions from the "dark region" of the plasma and the observed ion current is very small.

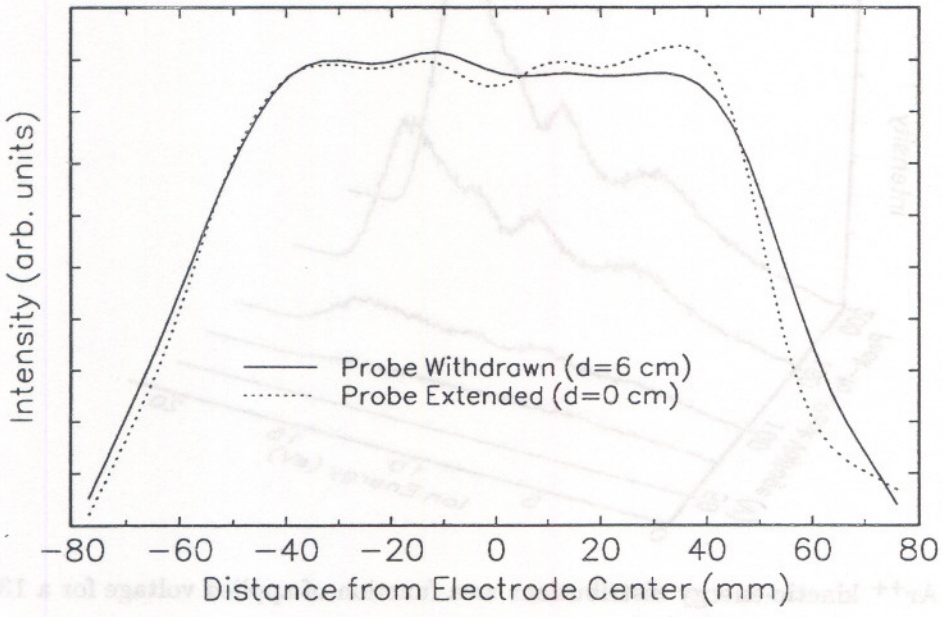

Figure 17. Effect of the mass spectrometer probe on the optical emission spatial profile (at 415.86 nm) with the probe extended and retracted for a 84 Pa (630 mTorr), 200 V argon plasma.

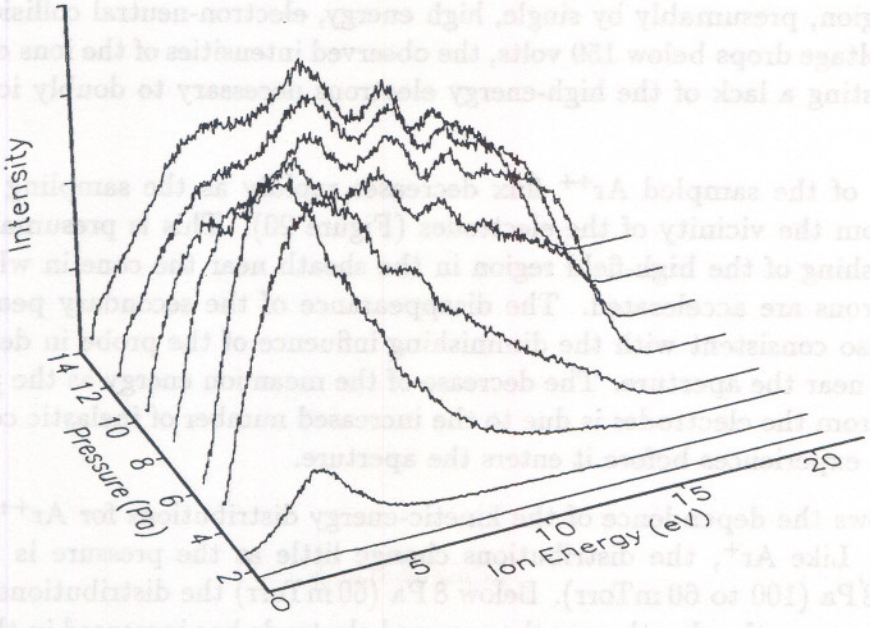

Figure 18. Ar^+ kinetic-energy distributions as a function of gas pressure for an argon plasma with d=0 and V_{pp}=200 V.

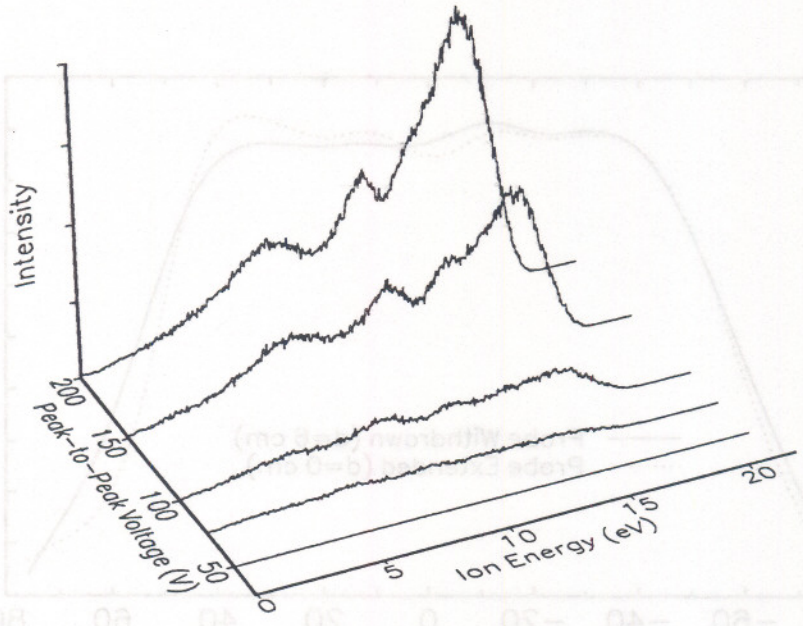

Figure 19. Ar^{++} kinetic-energy distributions as a function of applied voltage for a 13.3 Pa (100 mTorr) argon plasma with d=0

3.3.2 Ar^{++}

As seen in Figure 19, the ion kinetic-energy distributions for Ar^{++} also exhibit multiple peaks and a broad energy range. This indicates that Ar^{++} is formed in the sheath region, presumably by single, high energy, electron-neutral collisions. As the applied voltage drops below 150 volts, the observed intensities of the ions decrease rapidly suggesting a lack of the high-energy electrons necessary to doubly ionize an argon atom.

The intensity of the sampled Ar^{++} flux decreases rapidly as the sampling cone is withdrawn from the vicinity of the electrodes (Figure 20). This is presumably due to the diminishing of the high-field region in the sheath near the cone in which the ionizing electrons are accelerated. The disappearance of the secondary peaks as d increases is also consistent with the diminishing influence of the probe in defining a sheath region near the aperture. The decrease of the mean ion energy as the probe is moved away from the electrodes is due to the increased number of inelastic collisions which the ion experiences before it enters the aperture.

Figure 21 shows the dependence of the kinetic-energy distributions for Ar^{++} on the gas pressure. Like Ar^{+}, the distributions change little as the pressure is reduced from 13.3 to 8 Pa (100 to 60 mTorr). Below 8 Pa (60 mTorr) the distributions change significantly because the sheath near the powered electrode has increased in thickness such that plasma-sheath interface is positioned near the level of the sampling aperture.

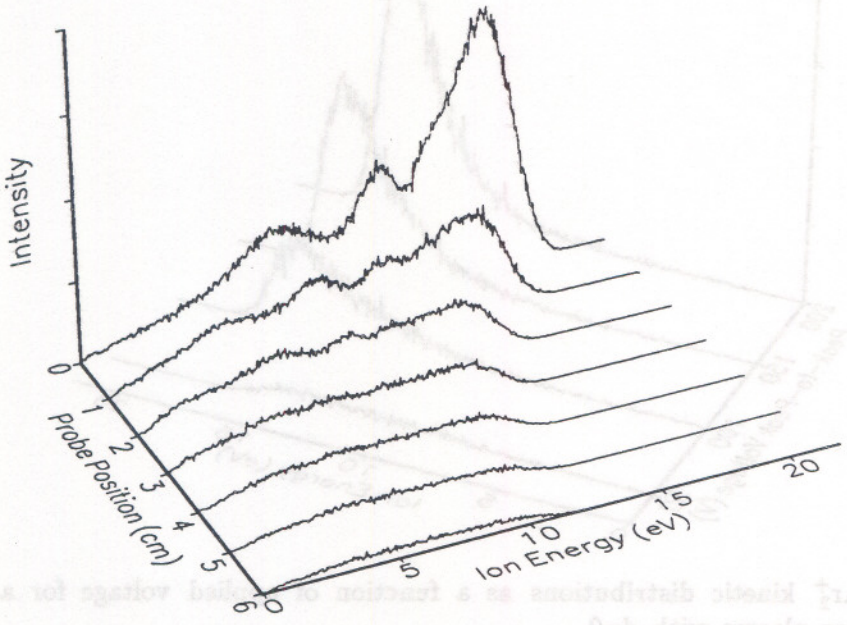

Figure 20. Ar^{++} kinetic-energy as a function of probe position for a 13.3 Pa (100 mTorr) argon plasma with V_{pp}=200 V

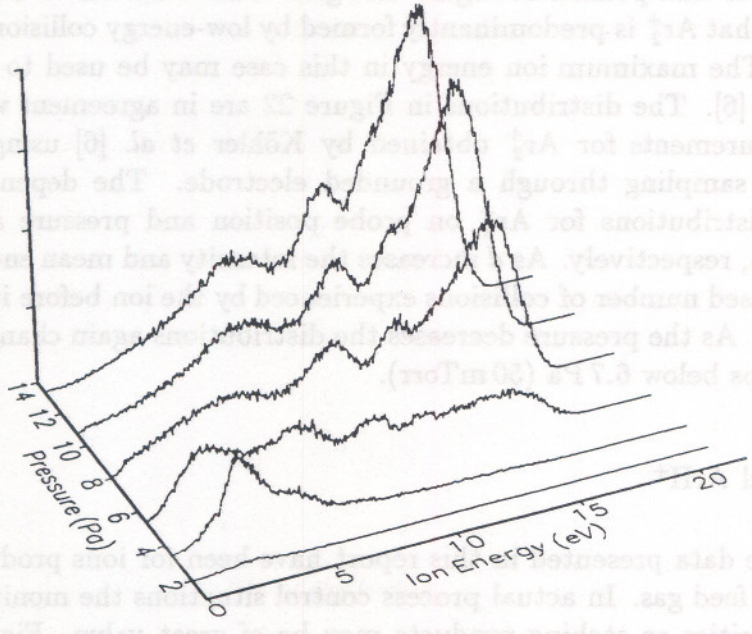

Figure 21. Ar^{++} kinetic-energy as a function of gas pressure for an argon plasma with V_{pp}=200 V and d=0

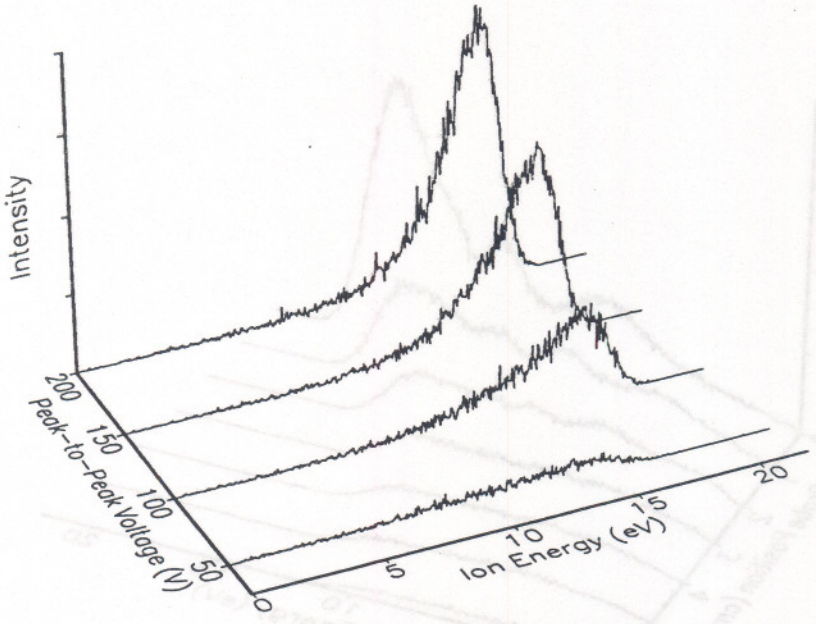

Figure 22. Ar_2^+ kinetic distributions as a function of applied voltage for a 13.3 Pa (100 mTorr) argon plasma with d=0

3.3.3 Ar_2^+

Unlike for Ar^+ or Ar^{++}, the measured Ar_2^+ kinetic-energy distributions (Figure 22) are much narrower and peaked at higher energies. This behavior is consistent with the expectation that Ar_2^+ is predominantly formed by low-energy collisions in the bulk of the plasma. The maximum ion energy in this case may be used to estimate the sheath potential [6]. The distributions in Figure 22 are in agreement with previous ion-energy measurements for Ar_2^+ obtained by Köhler *et al.* [6] using a spherical energy analyzer sampling through a grounded electrode. The dependence of the kinetic-energy distributions for Ar_2^+ on probe position and pressure are shown in Figures 23 and 24, respectively. As d increases the intensity and mean energy decrease due to the increased number of collisions experienced by the ion before it is extracted from the plasma. As the pressure decreases the distributions again change little until the pressure drops below 6.7 Pa (50 mTorr).

3.3.4 H_2O^+ and ArH^+

To this point the data presented in this report have been for ions produced directly from the plasma feed gas. In actual process control situations the monitoring of ions due to gas impurities or etching products may be of great value. Figure 25 is the kinetic-energy distribution for water ions sampled from a 200 V, 100 mTorr argon plasma. Water is always present to some degree in the discharge as an impurity. The

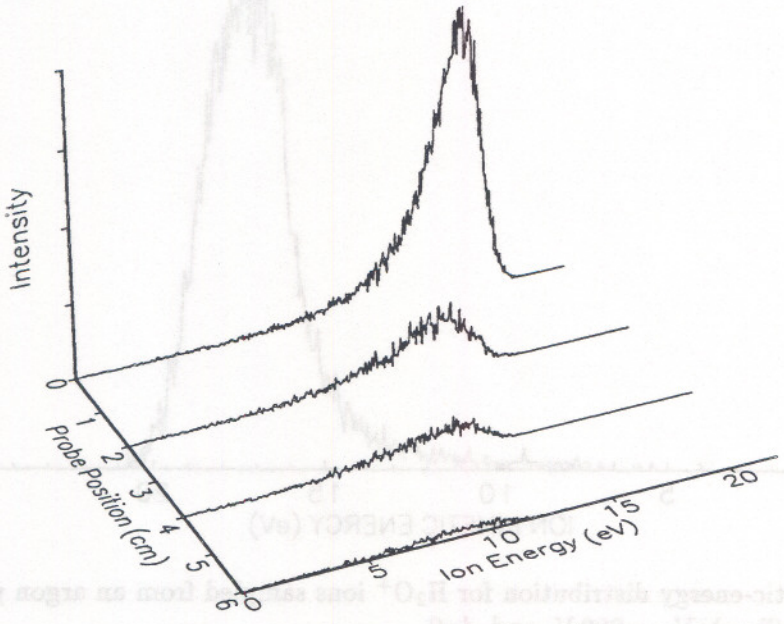

Figure 23. Ar_2^+ kinetic distributions as a function of probe position for a 13.3 Pa (100 mTorr) argon plasma with V_{pp}=200 V

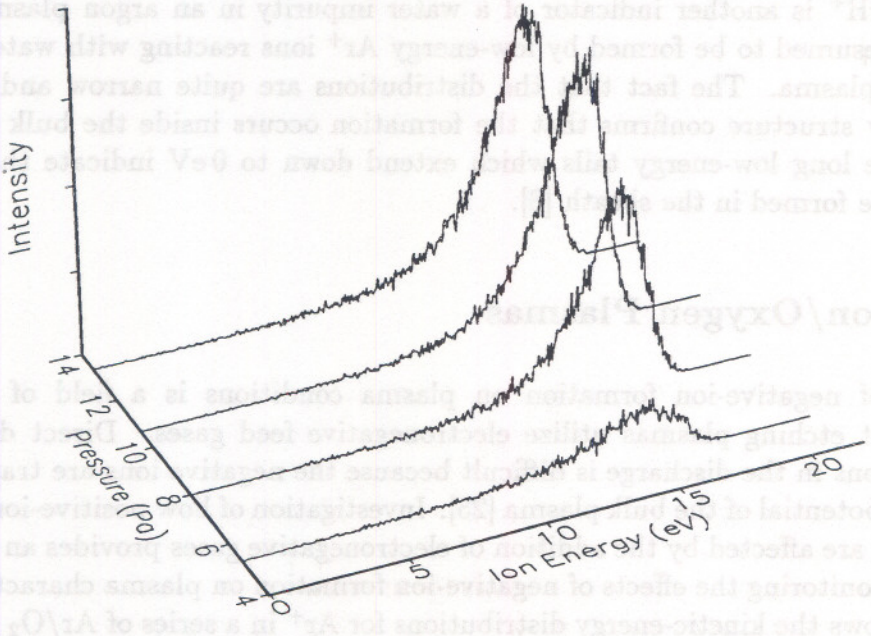

Figure 24. Ar_2^+ kinetic distributions as a function of gas pressure for an argon plasma with d=0 and V_{pp}=200 V

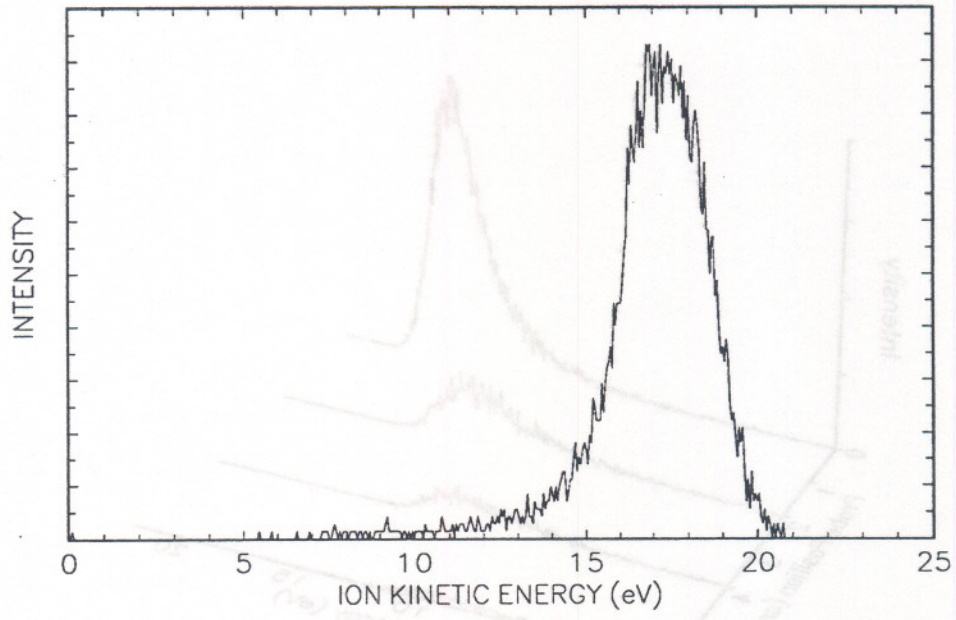

Figure 25. Kinetic-energy distribution for H_2O^+ ions sampled from an argon plasma with P=13.3Pa (100 mTorr), V_{pp}=200 V, and d=0

distribution in Figure 25 gives an indication of the ability of the BIT/RGA to detect weak ion fluxes resulting from impurities in the plasma.

Figure 26 shows several kinetic-energy distributions for ArH^+ as a function of pressure. ArH^+ is another indicator of a water impurity in an argon plasma since the ion is presumed to be formed by low-energy Ar^+ ions reacting with water vapor in the bulk plasma. The fact that the distributions are quite narrow and exhibit no secondary structure confirms that the formation occurs inside the bulk plasma. However, the long low-energy tails which extend down to 0 eV indicate that some ArH^+ may be formed in the sheath [8].

3.4 Argon/Oxygen Plasmas

The effect of negative-ion formation on plasma conditions is a field of interest because most etching plasmas utilize electronegative feed gases. Direct detection of negative ions in the discharge is difficult because the negative ions are trapped by the positive potential of the bulk plasma [25]. Investigation of how positive-ion energy distributions are affected by the addition of electronegative gases provides an indirect method of monitoring the effects of negative-ion formation on plasma characteristics. Figure 27 shows the kinetic-energy distributions for Ar^+ in a series of Ar/O_2 plasmas as a function of O_2 content. As oxygen is added to the argon discharge, substantial changes in the distributions are observed. When only a small amount of oxygen (2 %) is added to the argon a significant broadening of the distribution is observed and the

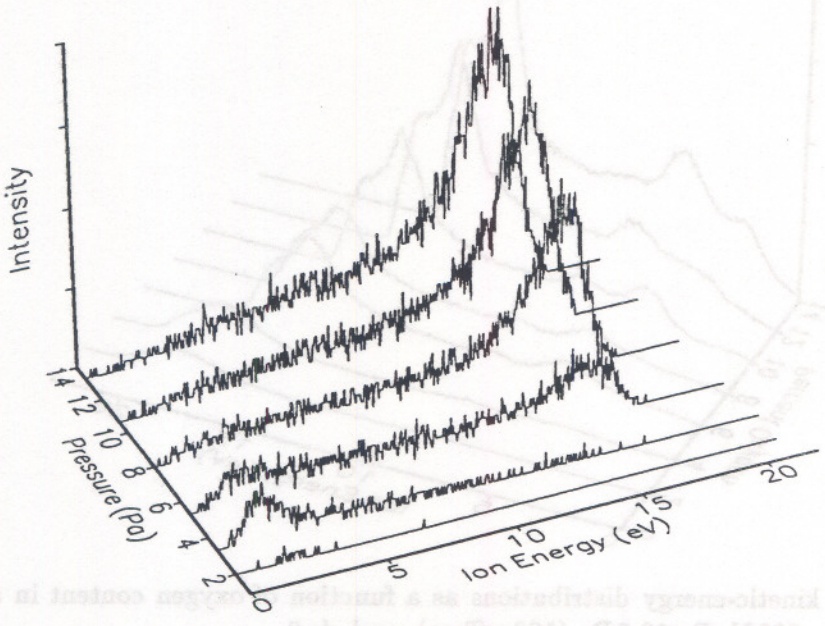

Figure 26. ArH^+ kinetic-energy distributions as a function of pressure for an argon plasma with V_{pp}=200 V and d=0

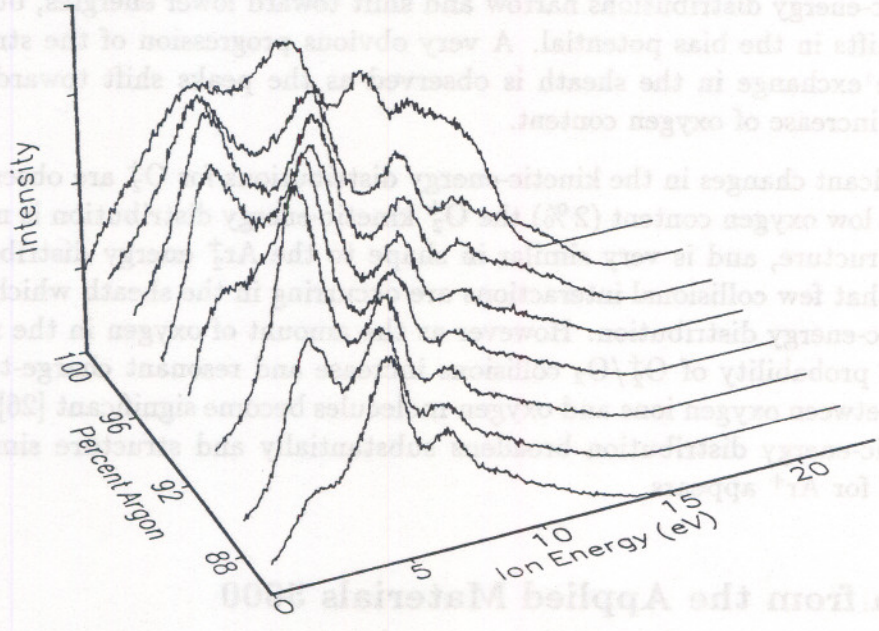

Figure 27. Ar^+ kinetic-energy distributions as a function of argon content in an Ar/O_2 plasma with V_{pp}=200 V, P=13.3 Pa (100 mTorr), and d=0. The oxygen content was varied from 0–14 %

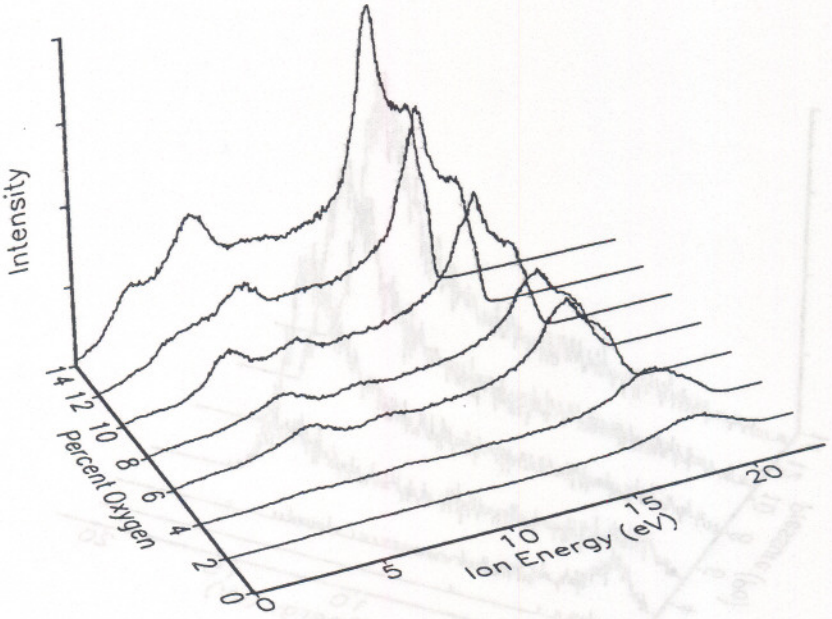

Figure 28. O_2^+ kinetic-energy distributions as a function of oxygen content in an Ar/O_2 plasma with V_{pp}=200 V, P=13.3 Pa (100 mTorr), and d=0.

maximum ion kinetic energy increases by approximately two volts. This increase is accompanied by a corresponding decrease in the self-bias potential due to the formation of negative ions in the plasma. As more oxygen is added to the discharge, the ion kinetic-energy distributions narrow and shift toward lower energies, but with only minor shifts in the bias potential. A very obvious progression of the structure due to charge exchange in the sheath is observed as the peaks shift toward lower energies with increase of oxygen content.

Equally significant changes in the kinetic-energy distributions for O_2^+ are observed in Figure 28. At low oxygen content (2 %) the O_2^+ kinetic-energy distribution is narrow, exhibits no structure, and is very similar in shape to the Ar_2^+ energy distributions. This implies that few collisional interactions are occurring in the sheath which affect the O_2^+ kinetic-energy distribution. However as the amount of oxygen in the reactor increases, the probability of O_2^+/O_2 collisions increase and resonant charge-transfer interactions between oxygen ions and oxygen molecules become significant [26]. Thus the ion kinetic-energy distribution broadens substantially and structure similar to that observed for Ar^+ appears.

3.5 Data from the Applied Materials 5000

Data was acquired using a BIT/RGA mounted on an Applied Materials 5000 etching reactor in order to verify that the conclusions drawn from the data obtained on the GEC reference cell are applicable to commercial reactors. Figure 29 shows a raw

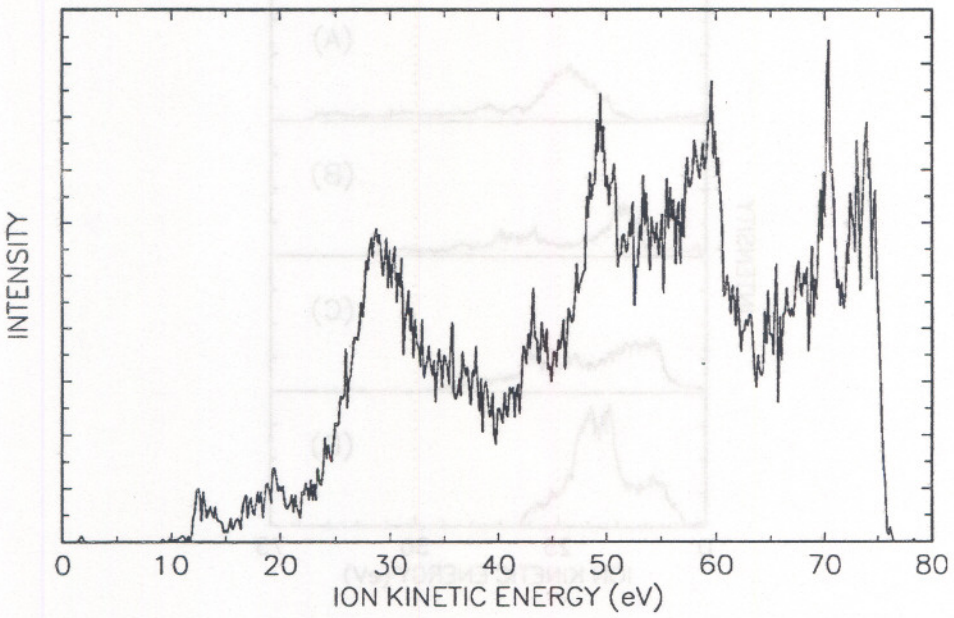

Figure 29. Raw Ar^+ kinetic-energy distribution obtained on an Applied Materials 5000 etcher for a 13.3 Pa (100 mTorr), 300 watt argon plasma.

Ar^+ kinetic-energy distribution for a 13.3 Pa (100 mTorr) argon plasma at a power setting of 300 W as measured by the reactor controller. The distribution extends to high kinetic-energy values ($\sim$ 75 eV) as a result of the high power levels in the reactor as compared with the GEC reference cell. Similar to the spectra obtained on the GEC cell, the distribution is broad and exhibits many secondary maxima due to charge-exchange interactions in the sheath. Note that this distribution exhibits a low-energy cut-off near 12 eV which is very similar to that observed in Figure 7 near 3.5 eV. This indicates that both instruments on both reactors experience the same surface charging effect discussed previously. All spectra shown in the remainder of the section will have their energy scales adjusted to account for this effect as described in Section 3.2.

It should be noted that the ion kinetic-energy distributions in the Applied Materials 5000 tended to change significantly with time, particularly when higher power levels were used. Day-to-day changes in the spectra observed in the Applied Materials 5000 reactor were much larger than those observed in the GEC reference cell, indicating that plasma conditions in the commercial reactor were changing more dramatically than in the research reactor. This can likely be attributed to the higher power levels utilized in the Applied Materials 5000 and to the presence of a silicon wafer on the powered electrode.

In Figure 30 the kinetic-energy distributions for Ar^+ as a function of reactor power setting (350 W, 250 W, 150 W, 50 W) are presented. As the power levels are decreased the maximum kinetic energy decreases in response to smaller applied rf voltages.

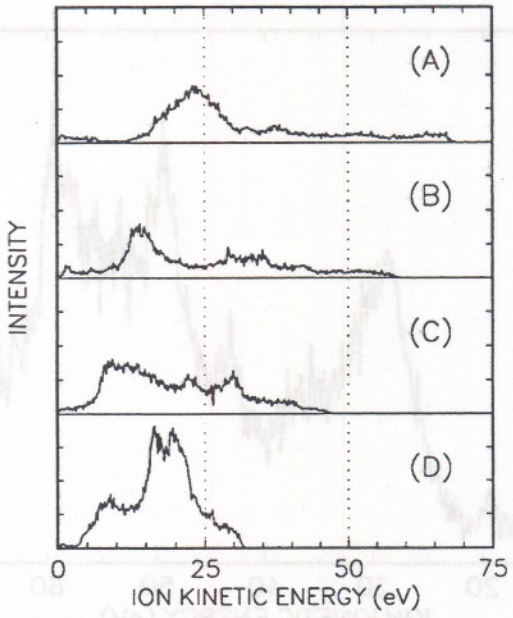

Figure 30. Ar^+ kinetic-energy distribution for a 13.3 Pa (100 mTorr) argon plasma at (A) 350 W, (B) 250 W, (C) 150 W, and (D) 50 W.

Secondary maxima are observed for all power levels, but these peaks do not exhibit the progressive shifting observed in Figure 15 as the peak-to-peak voltage was varied on the GEC reference cell.

Kinetic-energy distributions for Ar^{++} (as shown in Figure 31) are similar to the energy distributions for Ar^+. Each distribution is quite broad and exhibits secondary maxima. When compared with the Ar^+ distribution shown in Figure 30, it is observed that the Ar^{++} distributions have much lower intensities and extend to higher kinetic energies. ArH^+ (Figure 32) exhibits kinetic-energy distributions which are very similar to those obtained for Ar^{++} except the maximum energy is lower (< 70 eV).

Ar_2^+, which may provide an estimate of plasma potentials, is an extremely weak signal in the Applied Materials reactor. Only at the lower power levels ($\sim$ 50 W) is a significant Ar_2^+ ion flux observed. The kinetic-energy distribution for Ar_2^+ in a 13.3 Pa (100 mTorr), argon plasma is shown in Figure 33. Unlike the Ar_2^+ distributions obtained on the GEC reference cell, this distribution exhibits some structure, which perhaps indicates the presence of plasma non-uniformities.

The kinetic-energy distributions of etching and sputtering products may also be monitored by the BIT/RGA. In Figure 34 kinetic-energy distributions are shown for Si^+ ions sputtered from a silicon wafer by an argon plasma in the Applied Materials 5000. The signal levels are small, but adequate for detection. As the power level increases the maximum ion energies increase, but analysis of the low-energy portion of the distributions is hampered by low signal levels and low signal-to-noise ratios.

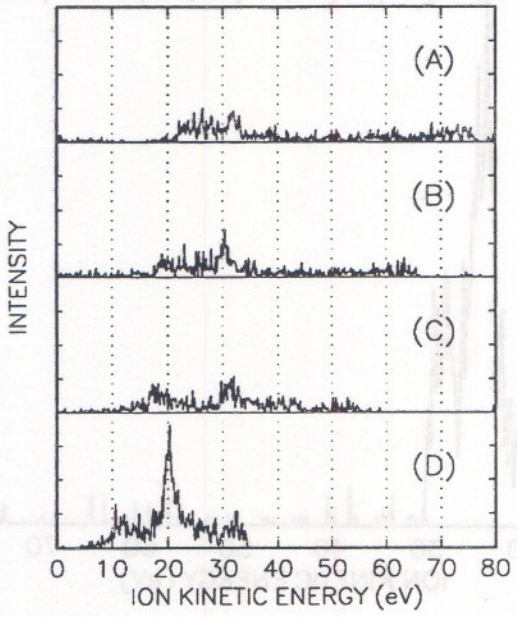

Figure 31. Ar^{++} kinetic-energy distribution for a 13.3 Pa (100 mTorr) argon plasma at (A) 350 W, (B) 250 W, (C) 150 W, and (D) 50 W.

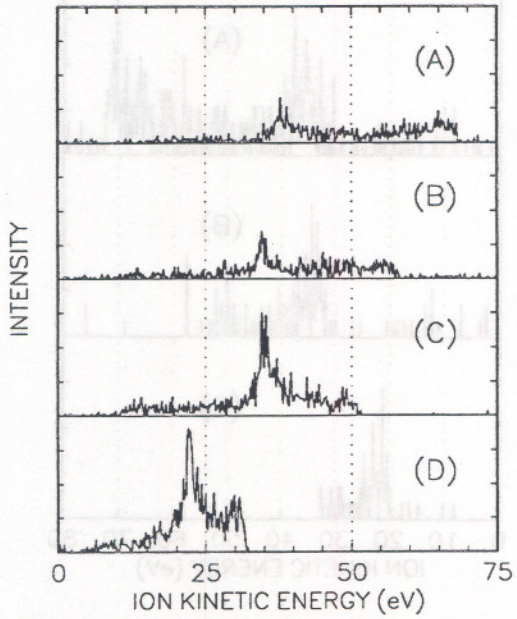

Figure 32. ArH^{+} kinetic-energy distribution for a 13.3 Pa (100 mTorr) argon plasma at (A) 350 W, (B) 250 W, (C) 150 W, and (D) 50 W.

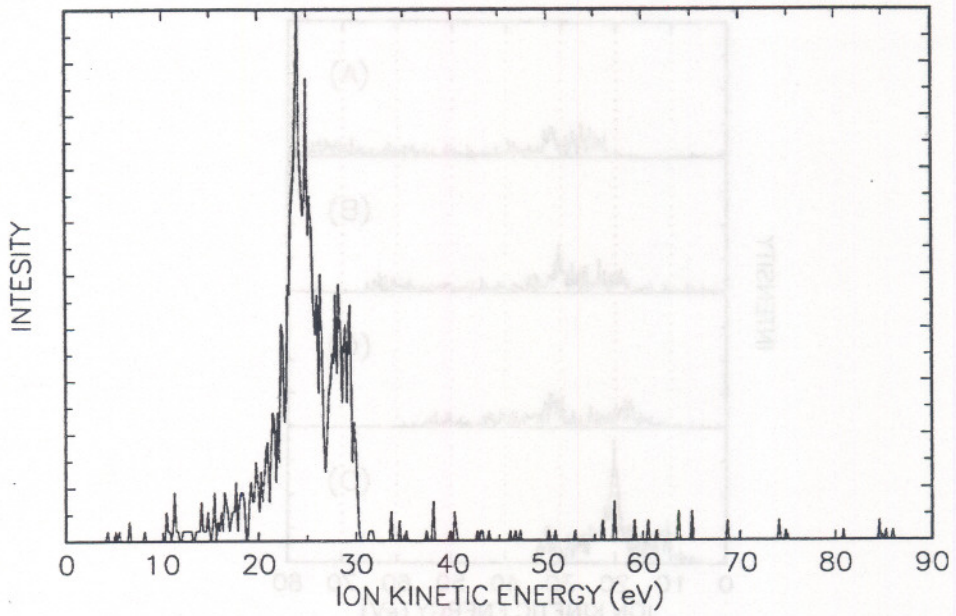

Figure 33. Ar_2^+ kinetic-energy distribution for a 13.3 Pa (100 mTorr) 50 W argon plasma.

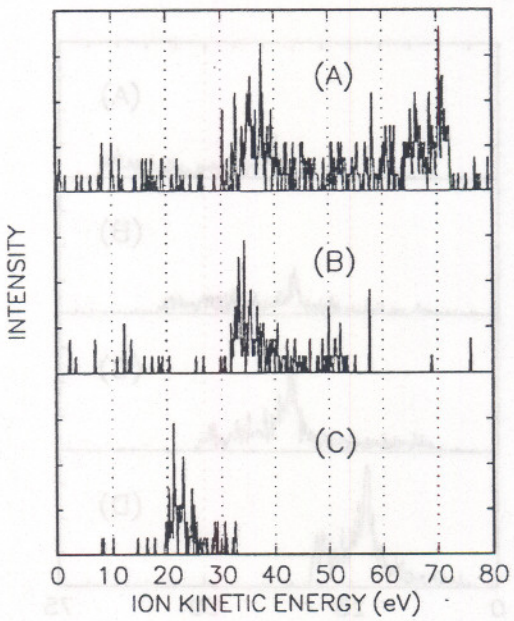

Figure 34. Si^+ kinetic-energy distribution sputtered from a silicon wafer by a 13.3 Pa (100 mTorr) plasma at (A) 350 W, (B) 150 W, and (C) 50 W.

In general the kinetic-energy spectra obtained from the larger, more complex, commercial etching reactor exhibited similar qualitative features when compared to the distributions obtained from the simpler, low-power GEC reference reactor. The observed "low-energy cut-off" indicates that the BIT/RGA operates in a similar manner on both reactors and that the calibration procedure described in the next section is applicable to both installations. However, the increased complexity of the distributions obtained on the Applied Materials 5000 indicates that more research needs to be done before the data obtained on high-power, commercial etchers can be interpreted in such a way that the BIT/RGA can be used as a control diagnostic.

4 Calibration Procedure

The calibration procedure presented here is meant to determine the "zero-energy point" of the ion kinetic-energy distributions measured by the BIT/RGA. Since no evidence was found to indicate that the "energy slope" or "kinetic-energy per channel" values ever changed, the determination of the zero-energy channel is sufficient for a calibration of the energy scale.

The procedure is based upon the knowledge that for an argon plasma with pressures near 100 mTorr, Ar^+ ions are sampled by the BIT/RGA with energies approaching 0 eV due to charge-exchange collisions in the sheath region [11, 12, 15, 16, 17]. Therefore the determination of the first channel at which an Ar^+ ion signal is observed determines the zero-energy point of the distribution once the 0.5 eV (FWHM) resolution of the energy analyzer is taken into consideration. If a different pass energy is used, then the corresponding energy resolution must be used for the calibration. The calibration procedure is straightforward and is listed below.

1. Obtain a kinetic-energy distribution for Ar^+ ions created in a 50–100 mTorr argon plasma. A vertical scale with sufficient sensitivity such that the maximum ion intensity is approximately full scale must be used, and the horizontal (energy) scale should be expanded (full scale $\sim$ 10 eV) around the zero energy point.

2. Determine the point on the kinetic-energy scale at which the Ar^+ signal first appears.
3. Add 0.25 eV (for a pass energy of 10 eV) to the kinetic-energy value determined in step 2 to account for the resolution of the energy analyzer.

4. The channel corresponding to the energy values derived in step 3 is then defined as the channel corresponding to kinetic energies of 0 ev. The distributions may then be shifted to account for this newly determined zero-energy point.

This technique exhibits an uncertainty of $\pm 0.3\,eV$ which is small compared to the fluctuations in kinetic-energy distributions observed on the Applied Materials 5000. It is important to note that this energy shift is sometimes time dependent, and is dependent upon applied voltages and ion flux magnitudes. The possible variation in the zero-energy point is obvious by comparing the spectra obtained on the GEC cell and the Applied Materials reactor (Figures 7 and 29, respectively) and by observing the increasing energy shift with increasing ion flux and energy in Figure 13. This suggests that for situations requiring accurate ion kinetic-energy measurements, that this procedure (or something similar) be used for each measurement.

5 Conclusions

From the data presented in this report it is clear that a significant amount of information is contained in data obtained by mass spectrometric and ion-energy analysis of a plasma. In the argon plasmas formed in the GEC reference cell, information about the identity, energy, formation mechanisms, intensities, and collisional interactions of plasma ions can be derived from the measured ion kinetic-energy distributions.

The BIT/RGA has been shown to be a suitable instrument for the monitoring of ions in an rf plasma discharge. The calibration of the energy scale is straightforward by analysis of the Ar^+ kinetic-energy distribution in an argon plasma. However, the long-term effects of repeated exposure to etching plasmas (such as Cl_2, BCl_3, HBr, etc.) requires further investigation.

The primary difficulty in the use of the BIT/RGA as a plasma diagnostic is in the interpretation of the data. In the well-characterized plasma system studied at NIST the fundamental processes occurring in the plasma are sufficiently well understood to allow a simple understanding of the basic features of the BIT/RGA data. However, even for these "simple" systems a complete understanding of all aspects of the ion kinetic-energy distributions is presently not possible. More research is required before a full interpretation of the measured ion kinetic-energy distributions from the GEC reference cell is possible.

When extended to the Applied Materials 5000, the difficulty in interpretation of the BIT/RGA is aggravated by the increased complexity of commercial etching reactors as compared with research reactors. The presence of the etching wafer in particular introduces a perturbation of the plasma which has not been adequately investigated. None of the basic investigations of the correlations between BIT/RGA measurements and plasma conditions have been performed on commercial reactors. The ion kinetic-energy distributions for an argon discharge in an Applied Materials 5000 were presented here only as examples of data. The basic knowledge required to

understand even the simplest plasmas is not presently available for the more complex, higher-power reactors.

These problems will be further compounded when the BIT/RGA is used to analyze reactive-gas plasmas. The more complicated gas-phase chemistry and the increased interactions with the wafer surface will dramatically increase the complexity of the data obtained by the BIT/RGA. At this time, the knowledge base is inadequate to fully interpret or understand this data. Additionally the correlations between mass spectrometric and ion energy data and the etch process are insufficiently defined to determine which portions of the BIT/RGA data are appropriate to monitor for real-time process control.

In order for the BIT/RGA to develop into a viable process control monitor a significant amount of research must be performed in the following areas:

1. A comprehensive study of neutral species, ions, and their kinetic energies in reactive gas plasmas must be performed. These studies should be done for CF_4, SF_6, BCl_3, Cl_2, HBr, O_2 and any mixtures which may be used in etching processes. These studies should be performed in simple, well-characterized rf discharge cells so that some understanding of the basic physical and chemical processes occurring in the plasma may be developed.

2. The measurements in Item 1 should be extended to include the presence of an etching wafer in the plasma. Particular attention should be paid to the perturbing effects on the data obtained in Item 1 and to any new gas-phase species being produced by interactions with the surface. These studies should also be carried out in simple, well-characterized rf discharge cells.

3. Comprehensive studies of BIT/RGA data obtained on commercial plasma etching reactors for simple plasma systems such as argon or helium should be performed. These results will provide an understanding of the BIT/RGA performance for that particular reactor which is required before any interpretation of more complex data is possible.

4. Studies similar to those listed in Item 2 should be performed on the commercial reactors.

5. Detailed correlations between etching results (i.e., rates, etching anisotropy, uniformity, surface damage, etch times, etc.) and the BIT/RGA data need to be determined. Once the portions of the BIT/RGA data which are relevant to the etching process are identified, techniques utilizing BIT/RGA data may be tailored to monitor the desired aspects of the etch process.

6. Correlations with other diagnostic techniques, such as optical emission and electric probes, need to be determined.

7. The BIT/RGA technique should be extended to provide time-resolved mass spectrometric data that is related to the phase of the applied rf voltages. This could prove to be a powerful diagnostic technique which may be sensitive to small changes in discharge conditions.

It is important to understand that the investigations discussed above must necessarily be empirical. From an application perspective, it is not practical to require a complete understanding of all the physical and chemical processes that influence the data obtained in these studies. If a sufficient degree of correlation is determined between the etching process and the control diagnostics, then it may be possible to define ranges of acceptable operating conditions as determined by the diagnostic measurements. At that point, the possibilities of feedback control, based upon the BIT/RGA data and other control diagnostics, should be explored.

5. REFERENCES

[1] B. Chapman, "Glow Discharge Processes", John Wiley and Sons, New York (1980).

[2] J. W. Coburn and H. F. Winters, *J. Vac. Sci. Technol.* **16**, 391 (1979).

[3] J. W. Coburn and H. F. Winters, *J. Appl. Phys.* **50**, 3189 (1979).

[4] J. M. Cook and K. G. Donohoe, *Solid State Technol.* 119, (April 1991).

[5] J. W. Coburn and E. Kay, *J. Appl. Phys.* **43**, 4965 (1972).

[6] K. Köhler, J. W. Coburn, D. E. Horne, E. Kay, and J. H. Keller, *J. Appl. Phys.* **57**, 59 (1985).

[7] K. Köhler, D. E. Horne, and J. W. Coburn, *J. Appl. Phys.* **58**, 3350 (1985).

[8] W. M. Greene, M. A. Hartney, W. G. Oldham, and D. W. Hess, *J. Appl. Phys.* **63**, 1367 (1988).

[9] H. Z. Sar-el, *Rev. Sci. Instrum.* **38**, 1210 (1967).

[10] S. G. Ingram and N. St. J. Braithwaite, *J. Phys. D: Appl. Phys.* **21**, 1496 (1988).

[11] J. Liu, G. L. Huppert, and H. H. Sawin, *J. Appl. Phys.* **68**, 3916 (1990).

[12] B. E. Thompson, K. D. Allen, A. D. Richards, and H. H. Sawin, *J. Appl. Phys.* **59**, 1890 (1986).

[13] M. F. Toups and D. W. Ernie, *J. Appl. Phys.* **68**, 6125 (1990).

[14] A. D. Kuypers and H. J. Hopman, *J. Appl. Phys.* **67**, 1229 (1990).

[15] A. Manenschijn, G. C. A. M. Janssen, E. von der Drift, and S. Raddelaar, *J. Appl. Phys.* **69**, 1253 (1991).

[16] Ch. Wild and P. Koidl, *Appl. Phys. Lett.* **54**, 505 (1989); *ibid., J. Appl. Phys.* **69**, 2909 (1991).

[17] G. Turban, B. Grollean, P. Launay, and P. Briand, *Revue Phys. Appl.* **20**, 609 (1985).

[18] N. Mutsukura and G. Turban, *Plasma Chem. Plasma Proc.* **10**, 27 (1990).

[19] B. A. Raby, *J. Vac. Sci. Technol.* **15**, 205 (1978).

[20] J. R. Roberts, J. K. Olthoff, R. J. Van Brunt, and J. R. Whetstone, *Advanced Techniques for Integrated Circuit Processing*, vol. 1392, pp. 428–436, Society of Photo-Optical Instrumentation Engineers, Bellingham, WA 1991.

[21] NIST/EPA/MSDC Mass Spectral Database, Ver. 2.0, Standard Reference Data, National Institute of Standards and Technology.

[22] E. W. McDaniel and E. A. Mason, *The Mobility and Diffusion of Ions in Gases* (John Wiley, New York) 1973, pp. 52–58.

[23] T. Makabe and H. Shinada, *J. Phys. D: Appl. Phys.* **18**, 2385 (1985).

[24] P. P. Ong and M. J. Hogan, *J. Phys. B: At. Mol. Phys.* **18**, 1897 (1985).

[25] L. J. Overzet, J. H. Beberman, and J. T. Verdeyen, *J. Appl. Phys.* **66**, 1622 (1989).

[26] C. W. Jurgensen, *J. Appl. Phys.* **64**, 590 (1988).